Petroleum Science (2018) 15:625–633
https://doi.org/10.1007/s12182-018-0243-0

ORIGINAL PAPER

Optimal activated carbon for separation of CO_2 from (H_2 + CO_2) gas mixture

Xiao-Xin Zhang[1] · Peng Xiao[2] · Chang-Yu Sun[2] · Gen-Xiang Luo[1] · Jia Ju[1] · Xiao-Rong Wang[1] · Hao-Xuan Wang[1] · Hao Yang[1]

Received: 5 January 2018 / Published online: 4 July 2018

Abstract
Seven types of activated carbon were used to investigate the effect of their structure on separation of CO_2 from (H_2 + CO_2) gas mixture by the adsorption method at ambient temperature and higher pressures. The results showed that the limiting factors for separation of CO_2 from 53.6 mol% H_2 + 46.4 mol% CO_2 mixture and from 85.1 mol% H_2 + 14.9 mol% CO_2 mixture were different at 20 °C and about 2 MPa. The best separation result could be achieved when the pore diameter of the activated carbon ranged from 0.77 to 1.20 nm, and the median particle size was about 2.07 μm for 53.6 mol% H_2 + 46.4 mol% CO_2 mixture and 1.41 μm for 85.1 mol% H_2 + 14.9 mol% CO_2 mixture. The effect of specific area and pore diameter of activated carbon on separation CO_2 from 53.6 mol% H_2 + 46.4 mol% CO_2 mixture was more significant than that from 85.1 mol% H_2 + 14.9 mol% CO_2 mixture. CO_2 in the gas phase can be decreased from 46.4 mol% to 2.3 mol%–4.3 mol% with a two-stage separation process.

Keywords Structure of activated carbon · Characteristic optimization · Separation · H_2 + CO_2 mixtures

1 Introduction

Hydrogen is becoming an important energy carrier to meet the needs of both the chemical industry and electrical generation (Momirlan and Veziroglu 2005; Yang et al. 2006). Hydrogen has two key advantages: low emissions and high calorific value. On the other hand, the synthetic gas originating from the steam reforming of natural gas followed by the water gas shift reaction is composed of (CO_2 and H_2) and a large amount of hydrogen can be obtained by purification of the synthetic gas (Hufton et al. 1999; Lee et al. 2007). Thus far, due to its merits of low cost, low-energy requirement, low pressure, and modest temperature, the method of adsorption separation has recently been received much interest. The critical factor for the method of adsorption separation is to find a suitable adsorbent with high selectivity for CO_2 and high CO_2 adsorption capacity.

There are several studies demonstrating that to maximise CO_2 uptake carbon materials need to have suitable structural features. Wickramaratne and Jaroniec (2013) synthesized phenolic resin-based carbon spheres obtained by a slightly modified Stober method, and found that it showed microporous carbon with fine pores (< 1 nm) and high specific surface area (2400 m^2/g) has high CO_2 capture at 0 °C and ambient pressures. The results of Yin et al. (2013) indicated that the surface properties of activated carbon had a little effect on CO_2 adsorption, while the volume of ultra-micropore (< 0.7 nm) had a significant effect on excess CO_2 adsorption capacity at pressure swing adsorption (PSA) conditions (0–20 °C, 0.01–0.10 MPa). Liu et al. (2017) synthesized nitrogen-enriched porous carbon spheres through a one-pot carbonization process and they proved that the carbon spheres which had a large amount of small micropores (< 1.0 nm) showed a good capacity to store CO_2 at 0.1 MPa and 25 °C. Adeniran et al. (2014) synthesized microporous carbons by heating a high carbon-

Edited by Xiu-Qin Zhu

✉ Xiao-Xin Zhang
zxx5266@126.com

[1] College of Chemistry, Chemical Engineering and Environmental Engineering, Liaoning Shihua University, Fushun 113001, China

[2] State Key Laboratory of Heavy Oil Processing, China University of Petroleum, Beijing 102249, China

containing metal salt under nitrogen, and their experimental results showed that 0.6–0.7 nm was advantageous for CO_2 uptake in a CO_2/N_2 system at 0.1 MPa and 25 °C. Kwac et al. (2016) emphasized the importance of graphitic pore size from 0.8 to 1.0 nm in CO_2 capture and selectivity against N_2. Coromina et al. (2015) found carbon with small micropores could satisfy the requirements of CO_2 uptake at low pressure and carbon with high surface area could satisfy the requirements for high pressure. In addition, there is some work (Cox and Mokaya 2017; Cao and Wu 2005) about the limiting factor for separating CO_2 from H_2 using carbon materials. Cox and Mokaya (2017) demonstrated that the porosity of the carbons, i.e., mesopores of size 2.5–5.0 nm and a few micropores, was favorable for CO_2 uptake at 25 °C and a pressure of 2–5 MPa, and their finding suggested that the presence of microporosity was a limiting factor in the CO_2 uptake capacity especially at high pressure (3–5 MPa). Cao and Wu (2005) simulated the separation of H_2/CO_2 via adsorption in activated carbon using grand canonical Monte Carlo simulations at 25 °C and 1–8 MPa and identified that the optimum pore sizes for the bulk mole fraction ratio of x_{CO_2}/x_{H_2} = 1:2 and x_{CO_2}/x_{H_2} = 1:8 were 1.48 nm and 1.18 nm, respectively.

In conclusion, a lot of work has been done on the limiting factors of CO_2 capture and storage with carbon materials, and a little experimental work has been done for the separation of (H_2 + CO_2) mixtures with activated carbon under high pressures. Considering the significance of structural features of the adsorbent for the selectivity of separating (H_2 + CO_2) mixtures with the adsorption method, it is necessary to study the effect of the structural features on separation performance of carbon materials at higher pressure. In this work, we first compared the selectivity for a (H_2 + CO_2) mixture using activated carbon KC-88 with those using metal–organic frameworks (MOFs) or membranes. Then, the effects of the specific surface area, micropore volume, pore diameter, and median particle size of the activated carbons were investigated for separating gas mixtures of (53.6 mol% H_2 + 46.4 mol% CO_2) and (85.1 mol% H_2 + 14.9 mol% CO_2) at about 2 MPa. The reusability of the activated carbons was also examined. These experimental data are useful for future applications of the separation of H_2/CO_2 gas mixtures with activated carbon or other porous materials at higher pressures.

2 Experimental section

2.1 Apparatus and material

The experimental apparatus used in this work has been described in detail in our previous papers (Liang et al. 2005; Zhang et al. 2014), and the schematic diagram is shown in Fig. 1.

Hydrogen (99.99%) and carbon dioxide (99.99%) were obtained from Beijing AP Beifen Gases Industry Company Limited. The typical synthesis gas from an integrated gasification combined cycle (IGCC) power station consists of approximately 60 mol% H_2 and 40 mol% CO_2 (Klara and Srivastava 2002; Jebraeel et al. 2011); a gas mixture of (53.6 mol% H_2 + 46.4 mol% CO_2) was prepared in our laboratory as the first component of feed gas. To observe the difference of separation performance in systems with different mole fraction ratios of CO_2 and the separation performance of activated carbon through a two-stage separation process, a gas mixture of (85.1 mol% H_2 + 14.9 mol% CO_2) was prepared as the second example of feed gas. The compositions of the feed gas and equilibrium gas were analyzed by a Hewlett-Packard 7890 gas chromatograph. The distilled water used has a conductivity of less than 10^{-4} S m^{-1}. Activated carbons were purchased from Hainuo Carbon Industry Co., Ltd., Shanghai (China), and Kecheng Guanghua New Technology Co., Ltd., Beijing (China). Before the experiment, the activated carbon samples (HN-1, HN-2, HN-3, HN-4, KC-92, KC-88, and Sigma) were dried to constant mass in a vacuum drying oven at 100 °C. The scanning electron microscope images of HN-1, HN-2, HN-3, HN-4, KC-92, KC-88, and Sigma were obtained from an FEI Quanta 200F SEM. The corresponding properties such as the specific surface area, micropore volume, and pore diameter, for these seven types of activated carbon were measured on a Micrometrics ASAP 2020 HD88 accelerated surface area and porosimetry system, and their median size and skeletal

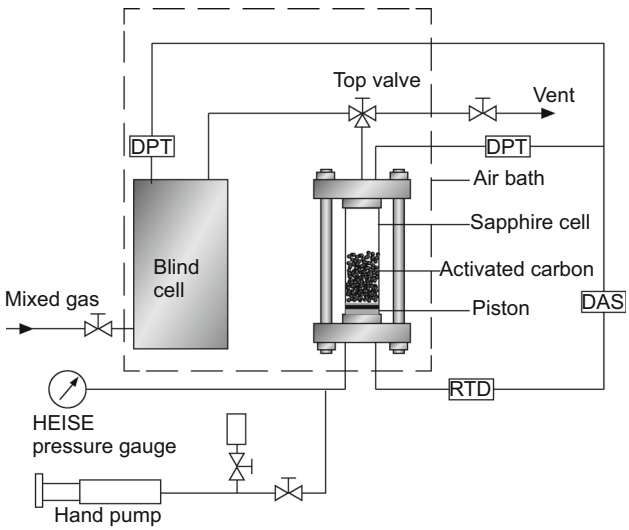

Fig. 1 Schematic diagram of the experimental apparatus. RTD, resistance thermocouple detector; DPT, differential pressure transducer; DAS, data acquisition system

density were measured with a HORIBA LA-950 laser particle size analyzer and a Quantachrome Ultrapycnometer 1000, respectively.

2.2 Procedures and data processing

The separation performance of activated carbons was evaluated according to the following procedure. At first, the sapphire cell was dismounted from the apparatus, washed with distilled water, dried, and loaded with a certain mass of activated carbon. Subsequently, the cell was installed into the apparatus again and connected to the blind cell, and the whole system was evacuated. Afterward, the top valve of the sapphire cell was closed and the blind cell was charged with the feed gas until the desired pressure was achieved. The air-bath temperature was then regulated to the desired value. When the temperature and the pressure of the gas mixture in the blind cell were stable at the specified value for a period of time, the stable pressure of the blind cell was recorded as P_1. Thereafter, the top valve of the sapphire cell was opened and the desired amount of feed gas originating from the blind cell was injected into the sapphire cell. When the pressure of the sapphire cell reached the desired value (recorded as P_0), the top valve was closed. Then, the adsorption separation experiment took place in the sapphire cell. After the pressure of the sapphire cell remained constant for a period of time, the separation process was deemed to have ended. The pressure of the residual gas in the blind cell and in the sapphire cell was recorded as P_2 and P_E, respectively. The equilibrium gas mixture in the sapphire cell was sampled under constant pressure by pushing the piston using a hand pump, and the corresponding composition was analyzed by HP 7890 gas chromatography.

Using the above procedures, the separation performance of activated carbons with different structures and the repeatability of activated carbons were investigated. The obtained data were processed as follows.

The total number of moles of the gas mixture (n_t) injected into the sapphire cell was calculated by the following formula:

$$n_t = \frac{P_1 V_t}{Z_1 RT} - \frac{P_2 V_t}{Z_2 RT}, \tag{1}$$

where P_1 was the initial pressure of the blind cell and P_2 was the residual pressure of the blind cell after injecting a certain amount of gas into the sapphire cell; V_t was the total volume of the blind cell plus the tubes connected to two cells; T was the system temperature; R was the universal gas constant; and the compressibility factors Z_1, Z_2 were calculated using the Benedict–Webb–Rubin–Starling equation of state.

The total number of moles of the equilibrium gas phase (n_E) in the sapphire cell was calculated by the following formula:

$$n_E = \frac{P_E V_g}{Z_E RT}, \tag{2}$$

where P_E was the equilibrium pressure of the sapphire cell; V_g was the volume of the equilibrium gas in the sapphire cell; Z_E was the compressibility factor corresponding to T, P_E, and the gas phase composition in the sapphire cell. The volume of the equilibrium gas in the sapphire cell was calculated by the following:

$$V_g = V_S - V_C, \tag{3}$$

where V_S was the effective volume of the sapphire cell and V_C was the skeleton volume of the activated carbon, which was further defined as follows:

$$V_C = \frac{m_c}{\rho_s}, \tag{4}$$

where m_c was the mass of the activated carbon for the separation experiments and ρ_s was the skeletal density of the activated carbon.

The total adsorbed number of moles of H_2 (n_1) and CO_2 (n_2) in the fixed bed of the activated carbon were calculated by the following::

$$n_1 = n_t \times z_1 - n_E \times y_1 \tag{5}$$

$$n_2 = n_t \times z_2 - n_E \times y_2, \tag{6}$$

where z_i and y_i were the molar fraction of H_2 and CO_2 in the feed gas and in the equilibrium gas phase, respectively. In addition, the corresponding molar fractions of H_2 and CO_2 in the pores of the activated carbon were defined as follows:

$$x_1 = \frac{n_1}{n_1 + n_2} \tag{7}$$

$$x_2 = \frac{n_2}{n_1 + n_2}. \tag{8}$$

The initial gas–solid ratio was calculated by the following:

$$S = \frac{22400 n_t}{V_C}. \tag{9}$$

The efficiency of separation was represented by selectivity, β, defined by the following (Cao and Wu 2005; Yang et al. 2009):

$$\beta = \frac{x_2/x_1}{y_2/y_1}. \tag{10}$$

The recovery of CO_2 in the adsorbed phase, R_2, was calculated by the following:

$$R_2 = \frac{n_2}{n_t \times z_2}. \quad (11)$$

The adsorption capacity for CO_2, M_2, was calculated by the following:

$$M_2 = (n_t - n_E) \times x_2. \quad (12)$$

3 Results and discussion

3.1 Comparison of the separation effect of different materials

The selectivities of H_2/CO_2 separation with different materials were first compared. The separation experiment with activated carbon KC-88 at 25 °C (named as run 1) was performed in this work with the feed gas composition of (53.6 mol% H_2 + 46.4 mol% CO_2), and the experimental results are tabulated in Table 1. For comparison, the simulated or experimental results with MOFs (Yang et al. 2009; Keskin and Sholl 2009), activated carbon (Cao and Wu 2005), or membranes (Richard et al. 2001; Guo et al. 2009) in the literature are also listed in Table 1, while the composition of the feed gas used in the literature is (50 mol% H_2 + 50 mol% CO_2). It can be seen that the selectivity, β, for MOF-5 (Keskin and Sholl 2009) and isoreticular metal–organic frameworks (IRMOFs) (Yang et al. 2009) (IRMOF-9, IRMOF-10, IRMOF-12, IRMOF-13, and IRMOF-14) are less than 100, while the selectivity, β, for membranes (microporous silica membrane and HKUST-1 membrane) (Richard et al. 2001; Guo et al. 2009) are less than 10 when the equilibrium pressure is approximately 1 MPa at 25 °C. The selectivity, β, in activated carbon (Cao and Wu 2005) is 45 at 25 °C and 2 MPa. However, for the activated carbon KC-88 used in this work, the selectivity, β, reaches 211 when the equilibrium pressure is 0.90 MPa at 25 °C. It is known that the price of MOFs and IRMOFs for use in separation experiments is very high and these materials are scarce. In comparison, the cost of activated carbon is very low and the production technology of activated carbon is so mature that it can be bought easily. However, there exist different structural features for different activated carbons. Suitable activated carbon that has a higher separation factor value must be chosen.

3.2 Effect of the structure of activated carbon

To examine the effect of the structure of activated carbon on the separation performance for (H_2 + CO_2) gas mixtures, seven types of activated carbon, namely HN-1, HN-2, HN-3, HN-4, KC-92, KC-88, and Sigma, were evaluated. The SEM images and their particle distribution are shown in Figs. 2, 3, and 4. The corresponding properties such as the specific surface area, micropore volume, pore diameter, median particle size, and skeletal density for the activated carbons are shown in Table 2. Among these activated carbons, HN-1, HN-2, HN-3, and HN-4 are derived from the same type of activated carbon, and have the same specific surface area, micropore volume, pore diameter, and skeletal density but with different particle sizes. The median particle sizes are 1.14, 1.41, 2.07, and 6.18 μm for HN-1, HN-2, HN-3, and HN-4, respectively. It is known that, in activated carbon, the particle size decides the utilization rate of the micropores, the pore diameter controls the probability of the gas molecules entering the pores of activated carbon, and the specific surface area and the pore volume decide the storage capacity for gas (Ozdemir and Schroeder 2009). That is, an optimum value exists for the pore diameter and the particle size to separate (H_2 + CO_2) gas mixtures, but, for the pore volume or specific surface area, the larger the better CO_2 uptake. In

Table 1 Comparison between the experimental and the literature values for separating (H_2 + CO_2) gas mixture with different materials

Type	Name	CO_2 in feed gas, mol%	Temperature, °C	Equilibrium pressure, MPa	β
Experiment (run 1)	KC-88	46.4	25	0.90	211
Simulation	MOF-5 (Yang et al. 2009; Keskin and Sholl 2009)	50	25	1.0	15
Simulation	IRMOF-11, IRMOF-13 (Yang et al. 2009)	50	25	1.0	< 100
Simulation	IRMOF-9 (Yang et al. 2009)	50	25	1.0	< 50
Simulation	IRMOF-10,12,14 (Yang et al. 2009)	50	25	1.0	< 10
Simulation	Activated carbon (Cao and Wu 2005)	50	25	2	45
Simulation	Microporous silica membrane (Richard et al. 2001)	50	25	2	3.5
Experiment	HKUST-1 membrane (Guo et al. 2009)	50	25	0.1	6.8

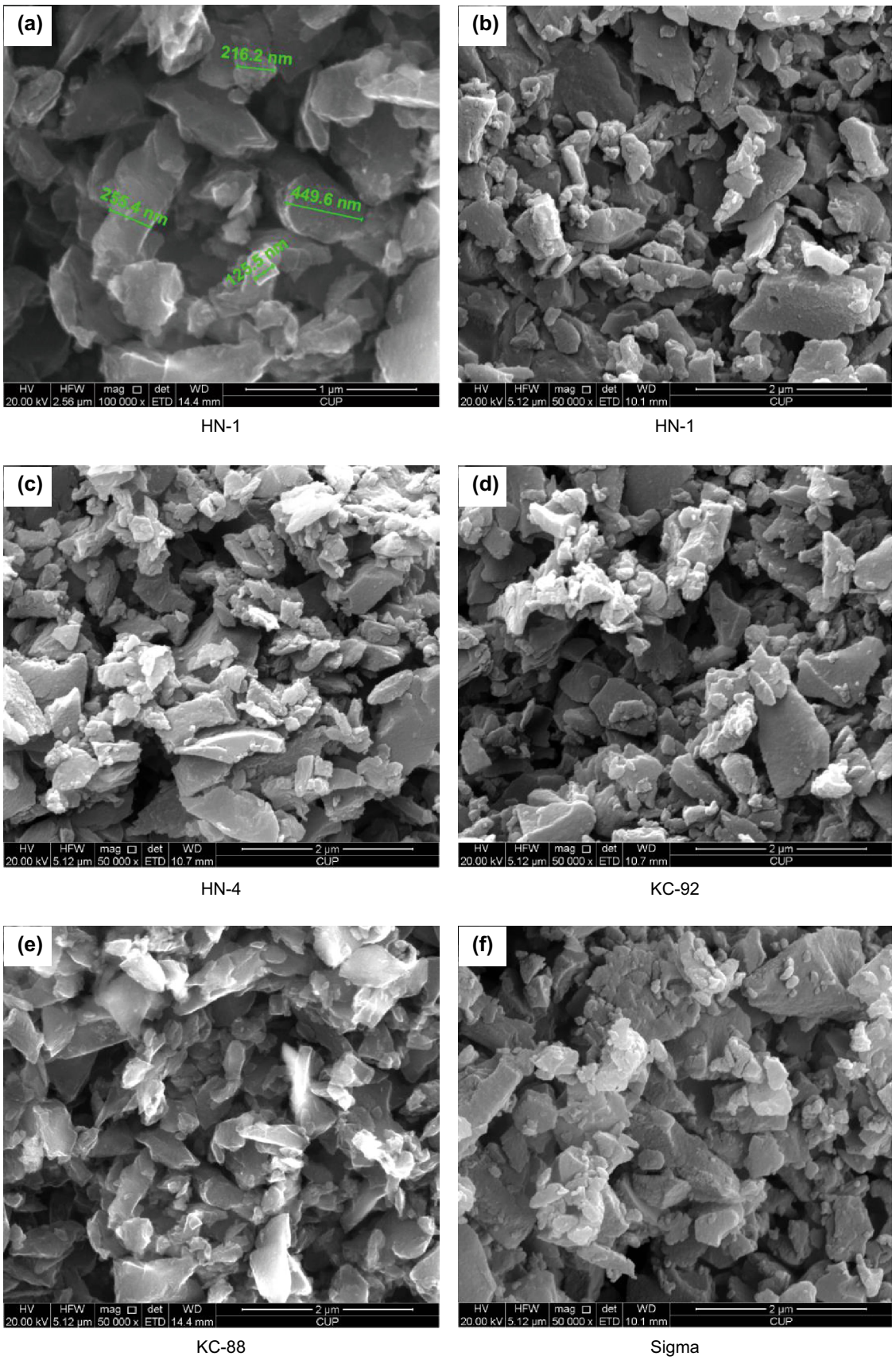

Fig. 2 SEM images of HN-1, HN-4, KC-88, KC-92, and Sigma

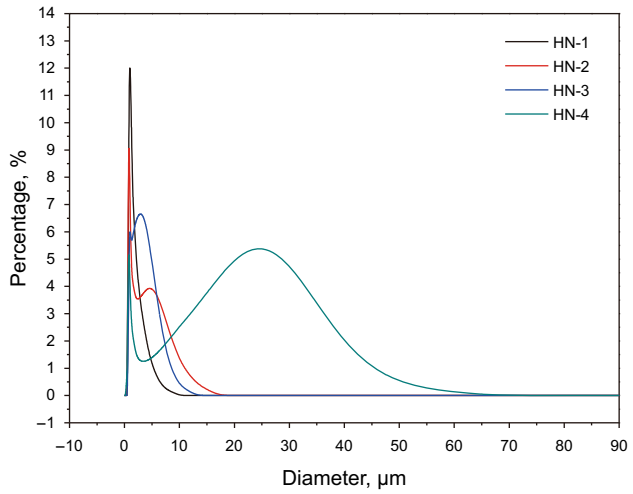

Fig. 3 Particle size distribution diagram of activated carbons (HN-1, HN-2, HN-3, and HN-4)

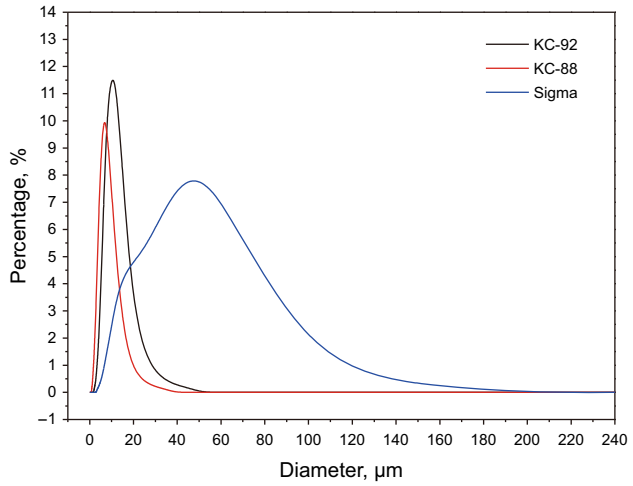

Fig. 4 Particle size distribution diagram of activated carbons (KC-88, KC-92, and Sigma)

this work, two gas mixtures were chosen to evaluate the effect of activated carbon's structure on the separation performance, which was (53.6 mol% H_2 + 46.4 mol% CO_2) and (85.1 mol% H_2 + 14.9 mol% CO_2). The separation results of seven types of activated carbon with these two feed gas mixtures (runs 2–15) are tabulated in Table 3. For this series of experiments, the temperature and initial pressure were 10 °C and approximately 2.0 MPa, respectively.

The separation performance for the (53.6 mol% H_2 + 46.4 mol% CO_2) feed gas mixture is first discussed. For HN-1, HN-2, HN-3, or HN-4 in which only the median particle size is different (runs 2–5), with the increasing particle size from 1.14 to 6.18 μm, the molar fraction of CO_2 in the equilibrium gas mixture, y_2, reached the minimum value (15.3%) and the adsorption capacity, M_2, for CO_2 reached maximum value (3.3 mmol/g) when the median particle size was 1.41 μm (HN-2); the selectivity, β, reached the maximum value (161) when the median particle size was 2.07 μm (HN-3). The experimental results showed that the median particle size controlled the CO_2 capture and selectivity for (53.6 mol% H_2 + 46.4 mol% CO_2) mixture when other structural features were constant, and the median particle size for optimal CO_2 capture and for optimal selectivity were different. Comparing the separation results of HN-1, HN-2, HN-3, and HN-4 for the (85.1 mol% H_2 + 14.9 mol% CO_2) (runs 9–15), y_2 reached the minimum value (2.9%) and the selectivity, β, reached the maximum value (181) when the median particle size was 1.41 μm; with the increasing of the particle size, M_2 changed slightly. Comparing the separation performance of HN-1, HN-2, HN-3, and HN-4 for (53.6 mol% H_2 + 46.4 mol% CO_2) and (85.1 mol% H_2 + 14.9 mol% CO_2), the effect of the particle size was more important for selectivity than CO_2 capture when the concentration of CO_2 was low.

Table 2 Structure information of seven types of activated carbon

Activated carbon	BET-specific surface area, m^2/g	*t*-plot micropore volume, cm^3/g	Pore diameter, nm	Median particle size, μm	Skeleton density, g/cm^3
HN-1	425	0.16	0.77	1.14	2.11
HN-2	425	0.16	0.77	1.41	2.11
HN-3	425	0.16	0.77	2.07	2.11
HN-4	425	0.16	0.77	6.18	2.11
KC-92	1442	0.50	0.93	9.39	2.00
KC-88	1716	0.44	1.20	6.02	2.52
Sigma	1410	1.49	1.69	32.80	1.63

Table 3 Separation results for two groups of (H_2 + CO_2) feed gas mixture with seven types of activated carbon when at 10 °C

Run no.	Activated carbon	P_0, MPa	P_E, MPa	S, v/v	y_2, %	x_2, %	R_2, %	β	M_2, mmol/g
(a) Feed gas mixture: 53.6 mol% H_2 + 46.4 mol% CO_2									
2	HN-1	2.13	1.37	422	18.2	96.4	74.9	121	3.0
3	HN-2	2.19	1.37	429	15.3	96.2	79.6	139	3.3
4	HN-3	2.11	1.37	395	21.0	97.7	69.7	161	2.7
5	HN-4	2.09	1.37	399	21.6	94.5	69.2	62	2.7
6	KC-92	2.17	1.33	401	14.2	95.6	81.4	130	3.4
7	KC-88	2.18	1.29	507	12.2	95.4	84.5	149	3.5
8	Sigma	2.07	1.35	304	22.1	92.1	68.9	41	2.9
(b) Feed gas mixture: 85.1 mol% H_2 + 14.9 mol% CO_2									
9	HN-1	1.91	1.53	369	3.0	66.0	83.6	63	1.0
10	HN-2	1.84	1.52	345	2.9	84.2	83.6	181	0.9
11	HN-3	1.92	1.54	354	3.0	71.9	83.1	82	0.9
12	HN-4	1.84	1.52	346	3.7	74.8	79.1	77	0.9
13	KC-92	1.86	1.51	329	3.1	71.9	82.9	81	0.9
14	KC-88	1.95	1.54	442	2.3	66.8	87.8	87	1.0
15	Sigma	1.89	1.54	267	4.3	71.7	75.7	57	0.8

P_0 the initial pressure in the sapphire cell; P_E the equilibrium pressure in the sapphire cell; S the initial gas–solid ratio; y_2 the molar fraction of CO_2 in the equilibrium gas phase; x_2 the molar fraction of CO_2 in the pores of the activated carbon; R_2 the recovery of CO_2 in the adsorbed phase; β the selectivity of CO_2 between the solid phase and the gas phase; M_2 the adsorption capacity for CO_2

Comparing the separation performance of KC-92, KC-88, and Sigma for (53.6 mol% H_2 + 46.4 mol% CO_2), y_2 reached a minimum value (12.2%), the selectivity β, and M_2 reached a maximum value (β = 149, M_2 = 3.5 mmol/g) for KC-88. Through comparing the structural information for KC-92, KC-88, and Sigma in Table 2, it could be probably confirmed that the specific surface area of KC-88 (1716 m^2/g) prompted y_2 to reach the minimum value (12.2%) and prompted M_2 to reach the maximum value (3.5 mmol/g), and the pore diameter (1.20 nm) or median particle size (6.02 μm) for KC-88 made selectivity reach the maximum value (β = 149). Comparing the structural features of HN-4 and KC-88, the median particle size of HN-4 (6.18 μm) and KC-88 (6.02 μm) were almost the same; the specific surface area and the pore diameter for HN-4 (425 m^2/g, 0.77 nm) and KC-88 (1716 m^2/g, 1.20 nm) differed greatly. Combining the difference of structural features for HN-4 and KC-88, the separation performance of HN-4 and KC-88 showed that the specific surface area decided the adsorption capacity for CO_2 and the pore diameter limited the selectivity for (53.6 mol% H_2 + 46.4 mol% CO_2), which was identical with the works of Cox and Mokaya (2017) about the presence of microporosity limiting the separation performance at higher pressure. Combining difference of the selectivity for HN-1, HN-2, HN-3, and HN-4 with increasing median particle size, the median particle size limited the selectivity of activated carbon for (53.6 mol% H_2 + 46.4 mol% CO_2). In conclusion, for (53.6 mol% H_2 + 46.4 mol% CO_2), the specific surface area limited the CO_2 capture, and the median particle size and the pore diameter limited the selectivity. The best separation performance is attained when the pore diameter is in the range of 0.77–1.20 nm and the median particle size is about 2.07 μm.

Table 3 also lists the separation performance of the activated carbons with the feed gas mixture of (85.1 mol% H_2 + 14.9 mol% CO_2) (runs 9–15). Comparing the separating performance of HN-4 and KC-88, the specific surface area and the pore diameter limited y_2 and selectivity β when median particle size was almost same. Comparing the separation performance of HN-3 and KC-92, y_2 and selectivity β were almost the same (HN-3: 3.0%, 82; KC-92: 3.1%, 81) when the specific surface area differed greatly (HN-3: 425 m^2/g and KC-92: 1442 m^2/g). Combining the variation of β, the median particle size limits the selectivity of activated carbon for (85.1 mol% H_2 + 14.9 mol% CO_2), and the best performance is reached when the median particle size is about 1.41 μm. Comparing the variation of y_2 and M_2 for seven activated carbon, the effect of specific area and pore diameter for (85.1 mol% H_2 + 14.9 mol% CO_2) are weaker than (53.6 mol% H_2 + 46.4 mol% CO_2), and better CO_2 capture can be reached when the pore diameter is in the range of 0.77–1.20 nm.

In conclusion, the best performance of (53.6 mol% H_2 + 46.4 mol% CO_2) and (85.1 mol% H_2 + 14.9 mol% CO_2) can be reached when the pore diameter is in the range of 0.77–1.20 nm and the median size is about 2.07 μm and

Table 4 Separation results for feed gas mixture of (53.6 mol% H_2 + 46.4 mol% CO_2) using activated carbon of KC-88 regenerated under different conditions

Run no.	Recovered temperature, °C	P_0, MPa	P_E, MPa	S, v/v	y_2, %	x_2, %	R_2, %	β	M_2, mmol/g
7	Fresh	2.18	1.29	507	12.2	95.4	84.5	149	3.5
16	20	2.09	1.37	491	15.0	95.5	77.8	120	3.0
17	20	2.13	1.47	495	23.9	86.9	62.2	21	2.4
18	40	2.13	1.39	498	18.6	89.5	72.3	38	2.8
19	60	2.10	1.36	492	16.5	91.7	75.6	56	2.9
20	80	2.12	1.34	494	14.5	92.6	79.0	74	3.0
21	100	2.17	1.36	509	12.3	95.0	82.6	138	3.2

The parameters with the same definitions as those in Table 3

1.41 μm, respectively. Comparing the simulation results of Cao and Wu (2005) who have confirmed that the optimized pore sizes for the bulk mole fraction ratio of x_{CO_2}/x_{H_2} = 1:2 and x_{CO_2}/x_{H_2} = 1:8 at 25 °C and 1–8 MPa are 1.48 nm and 1.18 nm, respectively, the experimental results in this work at 10 °C and about 2 MPa are reliable.

In addition, the feed gas composition of (85.1 mol% H_2 + 14.9 mol% CO_2) in runs 9–15 can be regarded as the composition of an equilibrium gas phase for feed gas (53.6 mol% H_2 + 46.4 mol% CO_2) in runs 2–8 after one stage of adsorption process. Therefore, the percent of CO_2 in the gas mixture of (53.6 mol% H_2 + 46.4 mol% CO_2) can be reduced to less than 4.3% after two stages of the adsorption process using activated carbon.

3.3 Regeneration of the activated carbon

To investigate the reuse of activated carbon for adsorption separation, separation experiments with KC-88 which was regenerated at different conditions with feed gas mixture of (53.6 mol% H_2 + 46.4 mol% CO_2) were performed at 10 °C and an initial pressure of 2.1 MPa. For run 7, fresh KC-88 was used; for run 16, KC-88 was regenerated by evacuating at 20 °C for 10 h; for runs 17–21, KC-88 was regenerated at different temperatures (20, 40, 60, 80, and 100 °C, respectively). The separation results for these experiments with the regenerated KC-88 are tabulated in Table 4. As observed from Table 4, for run 16, the molar fraction of CO_2 in the equilibrium gas y_2 reached 15.0% and the selectivity β reached 120, which was close to those with the fresh activated carbon system (run 7). For runs 17–21 with the regeneration temperature increasing from 20 to 100 °C, y_2 decreased from 23.89% to 12.3%, β increased from 21 to 138, x_2 increased from 86.9% to 95.0%, R_2 increased from 62.2% to 82.6%, and M_2 increased from 2.38 to 3.24 mmol/g. The separation performance of run 21 was similar to that of run 7. That is, the higher regeneration temperature is good for regenerating the activated carbon to be reused in subsequent separation experiments. Comparing the separation results of runs 16 and 20, y_2 in run 16 (15.0%) was almost the same as that in run 20 (14.5%), but x_2 and β in run 16 (x_2 = 95.5%, β = 120) were better than those in run 20 (x_2 = 92.6%, β = 74). Considering the separation results and the cost to regenerate the activated carbons with two different methods, it can be concluded that the used activated carbon is better regenerated by evacuating rather than by heating.

4 Conclusion

Seven types of activated carbon were examined to determine the limiting factors of the structure of activated carbons for separating gas mixtures (53.6 mol% H_2 + 46.4 mol% CO_2) and (85.1 mol% H_2 + 14.9 mol% CO_2) at 10 °C and about 2 MPa. The experimental data show that: for 53.6 mol% H_2 + 46.4 mol% CO_2, the pore diameter and median particle size limit the selectivity of activated carbons; for 85.1 mol% H_2 + 14.9 mol% CO_2, the median particle size limits the selectivity of activated carbons; the best separation performance can be attained for the two kinds of gas mixture when the pore diameter of the activated carbon ranges from 0.77 to 1.20 nm, and the median particle size is about 2.07 and 1.41 μm, respectively; the effect of specific area and pore diameter for latter mixture are weaker than the former mixture.

In addition, the molar fraction of CO_2 in the equilibrium gas mixture can be reduced from 46.4% to less than 4.3% in two stages using activated carbon. Over all, our findings are beneficial for separating industrial gas mixtures containing CO_2 using activated carbons under ambient temperature and higher pressures.

Acknowledgements Financial support was received from the Talent Scientific Research Fund of LSHU (No. 2016XJJ-015), the fund of the Liaoning Provincial Department of Education (No. L2017LQN005), and the National Natural Science Foundation of China (No. 21606120).

References

Adeniran B, Masika E, Mokaya R. A family of microporous carbons prepared via a simple metal salt carbonization route with high selectivity for exceptional gravimetric and volumetric post-combustion CO_2 capture. J Mater Chem A. 2014;35:14696–710. https://doi.org/10.1039/C4TA03565H.

Cao DP, Wu JZ. Modeling the selectivity of activated carbons for efficient separation of hydrogen and carbon dioxide. Carbon. 2005;43:1364–70. https://doi.org/10.1016/j.carbon.2005.01.004.

Coromina HM, Walsh DA, Mokaya R. Biomass-derived activated carbon with simultaneously enhanced CO_2 uptake for both pre and post combustion capture applications. J Mater Chem A. 2015;4:280–9. https://doi.org/10.1039/c5ta09202g.

Cox M, Mokaya R. Ultra-high surface area mesoporous carbons for colossal pre-combustion CO_2 capture and storage as materials for hydrogen purification. Sustain Energy Fuels. 2017;1:1414–24. https://doi.org/10.1039/c7se00300e.

Guo H, Zhu G, Hewitt IJ, et al. "Twin Copper Source" growth of metal organic framework membrane: $Cu_3(BTC)_2$ with high permeability and selectivity for recycling H_2. J Am Chem Soc. 2009;131:1646–7. https://doi.org/10.1021/ja8074874.

Hufton JR, Mayorga S, Sircar S. Sorption-enhanced reaction process for hydrogen production. AIChE J. 1999;45:248–56. https://doi.org/10.1002/aic.690450205.

Jebraeel G, Antonin C, Bahman T. Separation and capture of carbon dioxide from CO_2/H_2 syngas mixture using semi-clathrate hydrates. Chem Eng Res Des. 2011;89:1747–51. https://doi.org/10.1016/j.cherd.2011.03.008.

Keskin S, Sholl DS. Assessment of a metal organic framework membrane for gas separations using atomically detailed calculations: CO_2, CH_4, N_2, H_2 mixtures in MOF-5. Ind Eng Chem Res. 2009;48:914–22. https://doi.org/10.1021/ie8010885.

Klara SM, Srivastava RD. US DOE integrated collaborative technology development program for CO_2 separation and capture. Environ Prog Sustain Energy. 2002;21:247–53. https://doi.org/10.1002/ep.670210414.

Kwac K, Lee JH, Choi JW, et al. Computational analysis of pressure-dependent optimal pore size for CO_2 capture with graphitic surfaces. J Phys Chem C. 2016;120:3978–85. https://doi.org/10.1021/acs.jpcc.5b12404.

Lee KB, Beaver MG, Caram HS, et al. Novel thermal-swing sorption-enhanced reaction process concept for hydrogen production by low-temperature steam-methane reformation. Ind Eng Chem Res. 2007;46:5003–14. https://doi.org/10.1021/ie0701064.

Liang MY, Chen GJ, Sun CY, et al. Experimental and modeling study on decomposition kinetics of methane hydrates in different media. J Phys Chem B. 2005;109:19034–41. https://doi.org/10.1021/jp0526851.

Liu L, Xie ZH, Deng QF, et al. One-pot carbonization enrichment of nitrogen in microporous carbon spheres for efficient CO_2 capture. J Mater Chem A. 2017;5:418–25. https://doi.org/10.1039/C6TA0978K.

Momirlan M, Veziroglu TN. The properties of hydrogen as fuel tomorrow in sustainable energy system for a cleaner planet. Int J Hydrog Energy. 2005;30:795–802. https://doi.org/10.1016/j.ijhydene.2004.10.011.

Ozdemir E, Schroeder K. Effect of moisture on adsorption isotherms and adsorption capacities of CO_2 on coals. Energy Fuels. 2009;23:2821–31. https://doi.org/10.1021/ef801126a.

Richard V, Favre E, Tondur D, et al. Experimental study of hydrogen, carbon dioxide and nitrogen permeation through a microporous silica membrane. Chem Eng J. 2001;84:593–8. https://doi.org/10.1016/S1385-8947(01)00173-5.

Wickramaratne NP, Jaroniec M. Importance of small micropores in CO_2 capture by phenolic resin-based activated carbon spheres. J Mater Chem A. 2013;1:112–6. https://doi.org/10.1039/C2TA00388K.

Yang QY, Xu Q, Liu B, et al. Molecular simulation of CO_2/H_2 mixture separation in metal-organic frameworks: effect of catenation and electrostatic interactions. Chin J Chem Eng. 2009;17:781–90. https://doi.org/10.1016/S1004-9541(08)60277-3.

Yang YZ, Chang CH, Idriss H. Photo-catalytic production of hydrogen from ethanol over M/TiO_2 catalysts (M = Pd, Pt or Rh). Appl Catal B. 2006;67:217–22. https://doi.org/10.1016/j.apcatb.2006.05.007.

Yin GJ, Liu ZY, Liu QY, et al. The role of different properties of activated carbon in CO_2 adsorption. Chem Eng J. 2013;230:133–40. https://doi.org/10.1016/j.dej.2013.06.085.

Zhang XX, Liu H, Sun CY, et al. Effect of water content on separation of CO_2/CH_4 with active carbon by adsorption-hydration hybrid method. Sep Purif Technol. 2014;130:132–40. https://doi.org/10.1016/j.seppur.2014.04.028.